


Article

Low-Cost Nanostructured Coating of Anodic Aluminium Oxide Synthesized in Sulphuric Acid as Electrolyte

Florescia A. Bruera ^{1,2}, Gustavo R. Kramer ^{1,2}, María L. Vera ^{1,2} and Alicia E. Ares ^{1,2,*} 

¹ Instituto de Materiales de Misiones (IMAM), Consejo Nacional de Investigaciones Científicas y Técnicas (CONICET)-Universidad Nacional de Misiones (UNaM), Posadas 3300, Argentina; brueraflorencia@gmail.com (F.A.B.); guskramer@gmail.com (G.R.K.); veramalau@gmail.com (M.L.V.)

² Facultad de Ciencias Exactas, Químicas y Naturales (FCEQyN), Universidad Nacional de Misiones (UNaM), Posadas 3300, Argentina

* Correspondence: aares@fceqyn.unam.edu.ar; Tel.: +54-376-442-2186

Abstract: The anodic oxidation of aluminium is an electrochemical technique that allows obtaining nanostructures with easily adjustable morphology depending on the synthesis variables, for its application in medicine, engineering, biotechnology, electronics, etc. In this work, low-cost aluminium oxide nanostructured films were synthesized and morphologically characterized using two anodization steps in sulphuric acid, varying the concentration and temperature of the electrolyte and anodization voltage. The order of the porous matrix, pore diameter, interpore distance, pore density, thickness, and porosity were measured and statistically analyzed. The results showed that under the proposed conditions it is possible to synthesize low-cost nanoporous aluminium oxide films, with a short-range ordering, being the best ordering conditions 10 °C and 0.3 M sulphuric acid at 20 V and 5 °C and 2 M sulphuric acid at 15 V. Furthermore, it was determined that the pore diameter and the interpore distance vary proportionally with the voltage, that the pore density decreases with the voltage and increases with the concentration of the electrolyte, and that the thickness of the oxide film increases with electrolyte concentration, temperature, and anodization voltage.

Keywords: nanostructured anodic aluminium oxide; AA1050; statistics regression; sulphuric acid; morphological parameters



Citation: Bruera, F.A.; Kramer, G.R.; Vera, M.L.; Ares, A.E. Low-Cost Nanostructured Coating of Anodic Aluminium Oxide Synthesized in Sulphuric Acid as Electrolyte. *Coatings* **2021**, *11*, 309. <https://doi.org/10.3390/coatings11030309>

Academic Editor: Ingrid Milošev

Received: 5 February 2021

Accepted: 2 March 2021

Published: 9 March 2021

Publisher's Note: MDPI stays neutral with regard to jurisdictional claims in published maps and institutional affiliations.



Copyright: © 2021 by the authors. Licensee MDPI, Basel, Switzerland. This article is an open access article distributed under the terms and conditions of the Creative Commons Attribution (CC BY) license (<https://creativecommons.org/licenses/by/4.0/>).

1. Introduction

In recent years, great advances have been made in nanotechnology, especially in the area of nanomaterials, developing nanostructures with unique and versatile properties that are substantially improving the scientific, technological, and industrial sectors of the world [1].

Anodic aluminium oxide (AAO) is a nanomaterial that continues to be intensively studied and has shown its potential application in the fields of electronics, sensors, catalysis, separation, and biomedicine [2,3].

Nanoporous aluminium oxide films are obtained by anodic oxidation in acidic solutions [4], a simple and versatile electrochemical process that allows the synthesis of highly ordered nanostructures in a hexagonal arrangement of vertically aligned pores [5]. Today, the most widely used anodization technique is the two-step anodization developed by Masuda and Fukuda [6] and it consists of a first anodization, followed by the removal of the oxide layer formed to leave a periodic concave triangular pattern engraved on the surface of the metal, and a second anodization on the textured substrate surface to finally achieve a self-ordered growth of the pores [3,7].

It has recently been shown that the morphological parameters of the nanostructured AAO, such as the degree of arrangement of the porous structure, the pore diameter, the interpore distance, the pore density, the film thickness, and the porosity, strongly depend on the variables of the synthesis, such as nature, concentration, and temperature of the

electrolyte, together with the applied voltage and the anodization time [7–11]. Likewise, the purity of the aluminium used as substrate and the applied surface pretreatment to homogenize the surface have directly affected the ordering degree of the nanoporous arrangement [12–15].

AAO is normally synthesized using oxalic acid and sulphuric acid at temperatures below 20 °C, in a process that requires a long time (several hours or even days). However, at electrolyte temperatures above 20 °C, the oxide growth rate increases significantly due to greater ionic mobility and electrical conductivity of the electrolyte, which could reduce both synthesis times and costs [16,17].

For the synthesis of AAO films in sulphuric acid from high purity aluminium, various authors have defined as self-ordering regime: electrolyte temperature of 10 °C, 25 V, and several-day-duration of the anodization process [7,18,19]. Nevertheless, there is a certain range of voltage and temperature for each electrolyte that can be applied to anodize without burning, breaking, or excessively dissolving the oxide film even in the absence of an expensive cooling system [20].

On the other hand, the selection of the substrate for the anodic synthesis of nanostructures is an important factor, since the cost of the metal to be anodized increases depending on the degree of purity of the aluminium and the presence of impurities or alloys which affect the self-ordered development of the oxide film. So far, most research has focused on obtaining highly ordered anodic films using 99.99% and even 99.999% [21–24] pure aluminium substrate. However, the commercial AA1050 alloy (with 99.5% Al) [8,24–28] is a promising low-cost substrate alternative [4].

In previous works, the combined influence of synthesis variables on morphological parameters was exhaustively analyzed by using oxalic acid as electrolyte [11,15,29]. This type of analysis is still pending for other electrolytes, such as sulphuric acid, which would contribute to the optimization of resources in the anodic synthesis of OAA and facilitate the selection of the best synthesis conditions to obtain nanostructured films with a specific morphology as a function of the required application.

It should be noted that the independent effect of the anodization voltage, the concentration and the temperature of sulphuric acid on the characteristics of the oxide films were variable according to different studies carried out so far. For example, Sulka [7] determined that pore diameter and interpore distance depend only on voltage, while other authors also observed a significant effect of electrolyte concentration on pore diameter [10,30,31] and temperature on interpore distance [31].

Based on the above, the objectives of this work are to synthesize and morphologically characterize low-cost anodic aluminium oxide films, through two-step anodic oxidation of AA1050 aluminium using sulphuric acid as electrolyte, varying temperature, and anodization voltage, and then propose mathematical models that allow to explain and predict the relationship between morphological parameters and anodic synthesis variables.

Nanostructures surface images were taken by using optical microscopy and scanning electron microscopy, the latter were processed through the Fast Fourier Transform to qualitatively analyze the regularity of the pore arrangement [27,28,32] and regressions were performed with the quantitative data obtained from the morphological characterization by correlating morphological parameters and synthesis variables.

2. Materials and Methods

2.1. Substrate Material

The substrate used was a sheet of the commercial aluminium alloy AA1050 (min. 99.5% Al by weight), supplied by AMEX[®] S.A., Buenos Aires, Argentina. Samples of approximately 1 cm wide, 3 cm high, and 0.3 cm thick were cut, which were included in commercial acrylic (Subiton, San Fernando, Argentina) to isolate the edges and one of the faces and delimiting the exposed area of the samples to 3 cm².

2.2. Synthesis of AAO Coatings

2.2.1. Pre-Treatment of the Substrate Surface

The surface preparation of the substrate prior to the anodization was carried out applying the method detailed by Bruera et al. [15]. In this way, the following stages were carried out in succession: (i) grinding in a rotary plate polisher (Struers, Denmark) at 250 rpm, with SiC sandpaper of decreasing granulometry from # 280 to # 2500 (Doble A and Norton); (ii) polishing in rotary plate polisher (Struers, Ballerup, Denmark) at 250 rpm with diamond pastes of 6 μm (Prazis, Buenos Aires, Argentina) and 1 μm (Prazis, Buenos Aires, Argentina) for 30 min each on a cloth (Prazis, Buenos Aires, Argentina) using ethylene glycol (Biopack, Buenos Aires, Argentina) as a lubricant; (iii) electropolishing in ethanol 96% (Biopack, Buenos Aires, Argentina):85% phosphoric acid (Anedra, Buenos Aires, Argentina):water 3.5:4:2.5 V/V, vigorously stirring the solution at 40 °C with a magnetic stirrer under heating control (78HW-1, Arcano, China), at 60 V with limitation of current density in 0.25 A/cm² for 3 min, using two sources (TPR3003T, Atten, China) connected in series in potentiostatic mode and cathode of aluminium 99.999% (supplied by Aluar, Buenos Aires, Argentina) of 6 cm² of submerged area; and iv) attack in solution of 6% by weight of 85% phosphoric acid (Anedra, Buenos Aires, Argentina), 1.8% by weight of chromic acid (Cicarelli, Santa Fe, Argentina), 92.2% by weight of distilled water at 60 °C for 3 h. At the end of each pre-treatment stage, the specimens were cleaned with distilled water to remove any unwanted residue from the previous stage, sprayed with alcohol and dried with hot air.

2.2.2. Anodic Oxidation

Coatings were synthesized by anodic oxidation in two equal steps of 1 h each. Each anodizing step consisted in circulating direct current in potentiostatic mode, using two sources (TPR3003T, Atten, Shenzhen, China) connected in series and with magnetic stirring under heating control (78HW-1, Arcano, Nanjing, China) of the electrolyte. The AA1050 substrate (1 cm²) was used as the anode and a platinum plate (99.999%, Roberto Cordes SA, Buenos Aires, Argentina) of 12 cm² of exposed area was used as the cathode, both plunged in an electrolytic solution of sulphuric acid (Anedra, Buenos Aires, Argentina). After the first anodization step, the oxide layer produced was removed by chemically etching the test piece by immersion for 3 h in a solution of 6% by weight of phosphoric acid (Anedra, Buenos Aires, Argentina), 1.8% by weight of chromic acid (Cicarelli, Santa Fe, Argentina), and 92.2% by weight of water at 60 °C. On the same substrate the second anodizing step was carried out under identical conditions (as the first step).

Preliminary studies (not presented) showed that the range of levels of synthesis variables selected for sulphuric acid anodization is limited by excessive oxide dissolution and film breakdown, in the absence of a cooling system. Therefore, to synthesize low-cost aluminium oxide nanostructured films, the maximum temperature and voltage should be limited to 30 °C and 20 V for the 0.3 M sulphuric acid concentration, and 20 °C and 15 V for the concentration 2 M.

Thus, in this work, the synthesis variables in each oxidation (in both equal steps) were: electrolyte concentration (0.3 and 2 M), electrolyte temperature (5, 10, 20, and 30 \pm 2 °C) and anodization voltage (10, 12, 15, and 20 V).

2.3. Morphological Characterization of Coatings

The nanopores in the anodic films were characterized by scanning electron microscopy (SEM), using a SUPRA 40 (Carl Zeiss NTS GmbH, Buenos Aires, Argentina) equipment. The ordering of the porous structures, the average pore diameter (\bar{d}_p), the interpore distance (\bar{d}_i), the pore density ($\bar{\rho}$) and the porosity (\bar{P}) were determined from SEM micrographs with the free software ImageJ (1.50i version) [29,32–34].

To determine the ordering of the nanoporous structures, the Fast Fourier Transform (FFT) of the SEM images was used in an area of 3 μm^2 . \bar{d}_p was calculated from the area of each one of the pores identified in the SEM image with the analyze particles tool, assuming

a circular geometry. To estimate \overline{di} , twenty measurements were made from the center of one pore to the center of another, while for the determination of $\overline{\rho}$, the pore count per unit area tool was used. To calculate \overline{P} , four different areas of the SEM micrograph were analyzed with the analyze particles function to estimate the percentage (%) of the total oxide surface occupied by the pores [13].

The average thickness (\overline{e}) of the oxide films was determined by observing the cross-section of the sample under an optical microscope (EPIPHOT, Nikon, Tokyo, Japan), making ten measurements for each case. Previously, the cross-section of the samples was grinded and polished to facilitate the oxide film identification from the substrate in the microscope. This methodology was corroborated by SEM.

2.4. Statistic Analysis

The quantitative results obtained from the morphological characterization were analyzed by linear and non-linear regressions and by using the “Statgraphics Centurion XV.II” statistical software. The proposed adjustment models were selected taking into account the analysis of the results of the morphological characterization of the oxide coatings, the results of the multifactorial analysis of variance prior to regression (not shown) and the adjustment equations proposed in the literature considering the variables independently [19,20,22,35–37].

The mathematical models selected for the adjustment of the morphological parameters according to the synthesis variables are presented in Table 1, where \overline{dp} and \overline{di} are in nm, $\overline{\rho}$ in pores/cm², \overline{P} in percentage, and \overline{e} in μ m, C in M, T in °C and V in V. Such models were selected from the analysis of the results of the morphological characterization of the coatings and considering the adjustment equations proposed in the bibliography [7,10,35–39].

Table 1. Mathematical equations proposed for the adjustment of morphological parameters as a function of the synthesis variables.

Morphological Parameter	Adjustment Equation
\overline{dp}	$\overline{dp} = c \times C + t \times T + v \times V$ (1)
	$\overline{dp} = v \times V$ (2)
\overline{di}	$\overline{di} = c \times C + t \times T + v \times V$ (3)
	$\overline{di} = v \times V$ (4)
$\overline{\rho}$	$\overline{\rho} = c \times C + t \times T + \frac{v^2}{V^2}$ (5)
	$\overline{\rho} = c \times C + \frac{v^2}{V^2}$ (6)
\overline{e}	$\overline{e} = c \times C + t \times T + v \times V$ (7)
	$\overline{e} = c \times C + t \times T + v \times V + tv \times T \times V$ (8)
	$\overline{e} = c \times C + tv \times T \times V$ (9)
\overline{P}	$\overline{P} = c \times C + t \times T + v \times V$ (10)
	$\overline{P} = t \times T + v \times V$ (11)

The fidelity of the regression adjustment was estimated by the adjusted coefficient of determination (\overline{R}^2), an indicator of the variability explained by the proposed model. \overline{R}^2 expresses the percentage of variation in the response variable that is explained by its relationship with one or more predictor variables, adjusted for the number of predictors in the model. Thus, the higher the value of \overline{R}^2 , the better the proposed predictive model. While the aim of the regression analysis was to find an equation for \overline{dp} , \overline{di} , $\overline{\rho}$, \overline{P} , and \overline{e} that maximizes the value of \overline{R}^2 , the consistency between the predictions and the experimental results obtained were fundamental in the selection.

3. Results and Discussion

From the anodic synthesis conditions described above, nanoporous coatings of aluminium oxide were obtained with different ordering and \overline{dp} between 15.8 and 34 nm, \overline{di} between 28.6 and 56.0 nm, \overline{p} between 1.3×10^{11} and 3.7×10^{10} , \overline{e} between 3.9 and 58.9 μm , and \overline{P} between 14 and 34%. Table 2 shows the average values of the morphological parameters and the associated error for each condition of anodic synthesis.

Table 2. Average values of the morphological parameters of Anodic aluminium oxide (AAO) nanostructured coatings obtained in sulphuric acid as a function of concentration, temperature, and anodization voltage. The test pieces were named as follows: the letter S followed by a number, corresponding to the sulphuric acid and the value of the concentration in Molar; the letter T and the value of the electrolyte temperature in $^{\circ}\text{C}$ and the letter V together with the voltage value in volts. For example, S0.3 T10 V10 corresponds to an anodized test piece with two equal steps in 0.3 M sulphuric acid at 10°C and 10 V.

Sample	\overline{dp} (nm)	\overline{di} (nm)	\overline{p} (poros/cm ²)	\overline{e} (μm)	\overline{P} (%)
S0.3 T10 V10	21.0 ± 3.3	29.9 ± 4.4	$1.1 \times 10^{11} \pm 1.2 \times 10^8$	3.9 ± 0.55	28.7 ± 2.0
S0.3 T10 V15	27.8 ± 3.3	40.9 ± 4.2	$6.6 \times 10^{10} \pm 7.7 \times 10^8$	6.4 ± 0.45	26.0 ± 1.8
S0.3 T10 V20	34.0 ± 3.2	56.0 ± 6.2	$4.3 \times 10^{10} \pm 2.1 \times 10^9$	9.6 ± 0.55	29.8 ± 4.5
S0.3 T20 V10	21.4 ± 3.1	29.9 ± 4.4	$1.1 \times 10^{11} \pm 3.7 \times 10^8$	6.0 ± 0.71	26.1 ± 0.3
S0.3 T20 V15	27.3 ± 3.3	42.1 ± 7.0	$6.6 \times 10^{10} \pm 1.4 \times 10^9$	10.3 ± 1.06	23.5 ± 3.1
S0.3 T20 V20	34.2 ± 3.1	51.9 ± 4.7	$4.4 \times 10^{10} \pm 6.7 \times 10^8$	20.0 ± 0.41	27.2 ± 0.6
S0.3 T30 V10	21.2 ± 2.8	31.3 ± 4.4	$1.1 \times 10^{11} \pm 2.0 \times 10^9$	9.1 ± 0.4	34.0 ± 0.5
S0.3 T30 V15	26.3 ± 2.8	42.3 ± 7.5	$6.1 \times 10^{10} \pm 1.4 \times 10^9$	20.6 ± 1.0	32.6 ± 0.4
S0.3 T30 V20	29.7 ± 2.7	49.9 ± 4.7	$4.2 \times 10^{10} \pm 3.1 \times 10^8$	32.3 ± 0.8	27.5 ± 0.2
S2 T5 V10	15.8 ± 2.6	26.5 ± 3.8	$1.6 \times 10^{11} \pm 1.2 \times 10^9$	5.9 ± 0.2	14.0 ± 0.4
S2 T5 V12	19.9 ± 2.9	30.9 ± 4.6	$1.3 \times 10^{11} \pm 2.2 \times 10^8$	9.7 ± 0.2	21.0 ± 0.7
S2 T5 V15	20.4 ± 2.2	34.7 ± 5.0	$9.2 \times 10^{10} \pm 4.5 \times 10^8$	17.9 ± 0.4	19.9 ± 3.0
S2 T10 V10	18.4 ± 3.3	28.6 ± 5.2	$1.5 \times 10^{11} \pm 2.1 \times 10^9$	10.2 ± 0.2	16.3 ± 1.7
S2 T10 V12	19.9 ± 2.2	30.2 ± 3.8	$1.1 \times 10^{11} \pm 3.0 \times 10^9$	15.5 ± 0.1	27.1 ± 0.6
S2 T10 V15	22.4 ± 3.6	35.5 ± 4.4	$8.7 \times 10^{10} \pm 1.7 \times 10^9$	22.0 ± 0.7	28.9 ± 0.4
S2 T20 V10	18.2 ± 2.3	28.1 ± 4.1	$1.3 \times 10^{11} \pm 2.3 \times 10^9$	19.4 ± 0.3	20.3 ± 0.2
S2 T20 V12	17.9 ± 3.1	32.7 ± 4.9	$1.2 \times 10^{11} \pm 2.9 \times 10^9$	26.8 ± 0.4	21.6 ± 0.4
S2 T20 V15	23.2 ± 2.4	37.2 ± 4.7	$8.6 \times 10^{10} \pm 2.5 \times 10^8$	58.9 ± 0.3	25.7 ± 2.6

3.1. Ordering of the AAO Porous Film

Figures 1 and 2 present the SEM images of the nanostructured oxide coatings obtained by anodic oxidation of AA1050 in 0.3 and 2 M sulphuric acid solution, respectively, at different temperatures and voltages. In each case, the respective FFTs are presented below the micrographs.

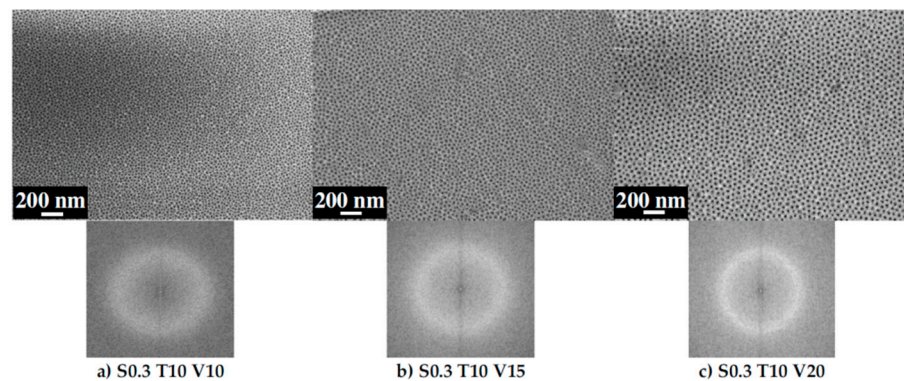


Figure 1. Cont.

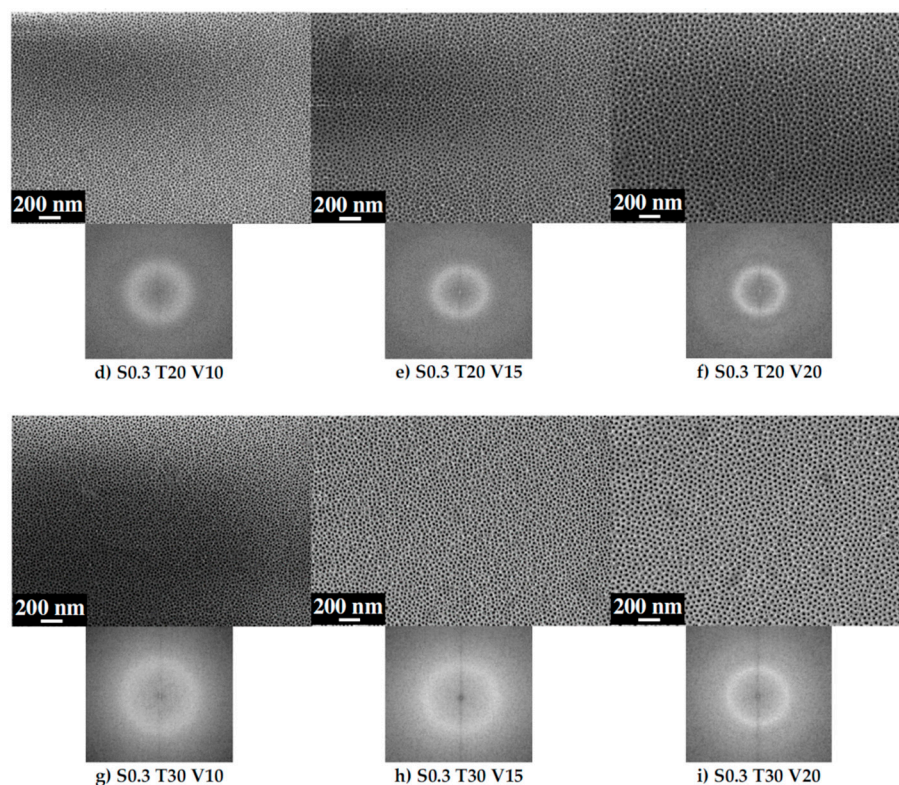


Figure 1. SEM images with their Fast Fourier Transforms of AA1050 oxide nanostructured films obtained in 0.3 M sulphuric acid and at different anodizing temperatures and voltages.

It can be observed that the samples synthesized in 0.3 M sulphuric acid at 10, 15, and 20 V showed a slight decrease in the ordering of the porous matrix as the synthesis temperature is increased by 10, 20 and 30 V. In general, a diffuse disk-shaped FFT pattern is observed (Figure 1a–c) which grows wider with increasing temperature (Figure 1g–i), indicating that there is no additive trend in the configurations of periodic pores due to poor ordering. This could be explained considering that high electrolyte temperatures increase the growth rate of the oxide and, consequently, decrease the time required for the self-organization process of the porous matrix [27].

On the other hand, for each of the different electrolyte temperatures, a slight increase in pore matrix ordering was observed as the anodization voltage increases. Evidence of this is the transformation of the diffuse disk-shaped FFT pattern, observed in the films synthesized with the lowest levels of temperature and voltage (Figure 1a,d,g), into a sharper and more defined FFT pattern, approaching the ring shape characteristic of a more ordered structure (Figure 1c,f,i). This result coincides with that observed by Sulka [7], who identified improvements in the ordering arrangement of the pores with the increase in voltage for the anodizations carried out in sulphuric acid.

The best order of the synthesized OAA films with two anodization steps in 0.3 M sulphuric acid, during 1 h and at different temperatures and voltages was obtained at 10 °C and 20 V (Figure 1c), being a non-ideal and short-range ordering per unit surface.

Furthermore, the results of Figure 1 presented the same trend as those reported in the literature within the experimental range 10–25 V [7,18,19]. In these works, the self-ordering regime was determined at 10 °C and 25 V, using sulphuric acid 0.3 M, aluminium of high purity, and an anodization time of several days.

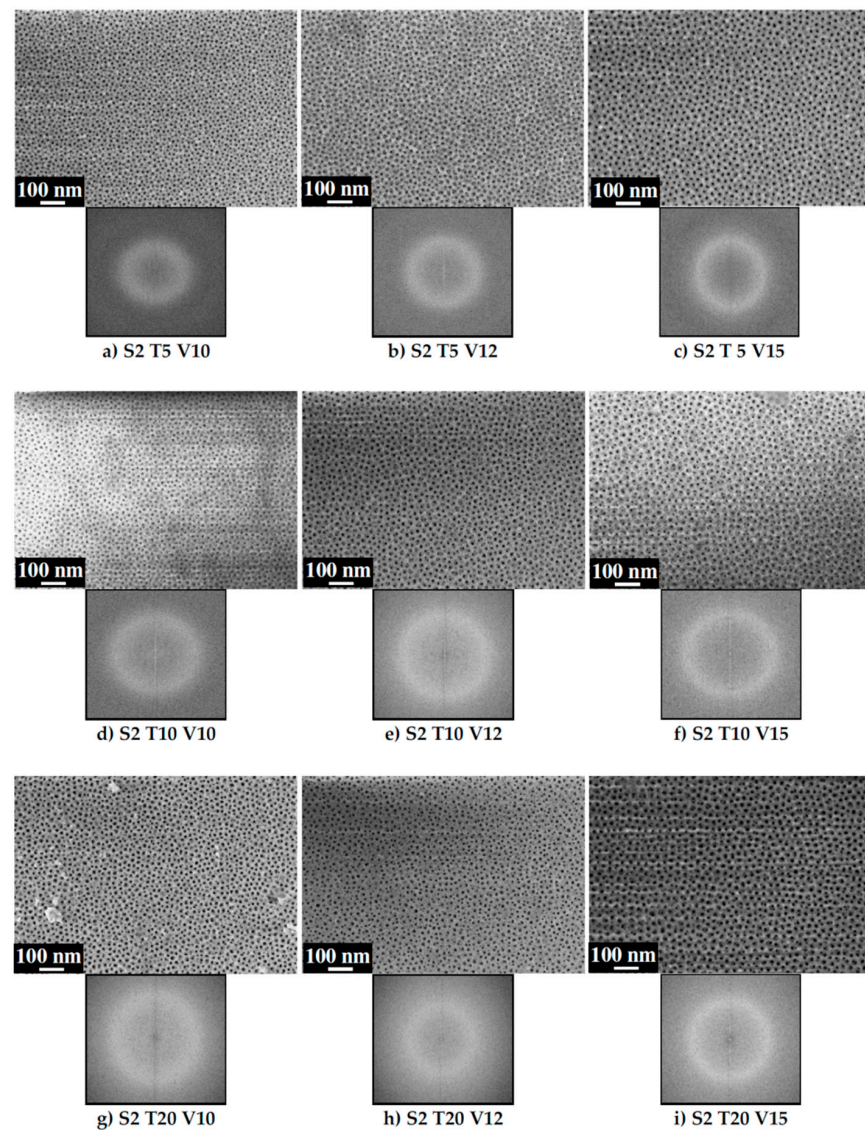


Figure 2. SEM images with their Fast Fourier Transforms of AA1050 oxide nanostructured films obtained in 2 M sulphuric acid and at different anodizing temperatures and voltages.

Figure 2 shows that, the variation in the degree of arrangement of the pore matrix of the anodized 2 M sulphuric acid samples with respect to the temperature and voltage, displayed a similar behavior to that of the anodized 0.3 M sulphuric acid. In other words, a decrease in the degree of ordering of the porous matrix with increasing temperature and a slight increase with voltage can be observed in Figure 2. For example, at 5 °C and 10 V (Figure 2a) the FFT pattern presents the shape of a diffuse disk that broadens with increasing temperature and becomes less and less defined (Figure 2g). Further, this FFT pattern (Figure 2a) becomes sharper with the increase in anodization voltage (Figure 2c). Therefore, the best ordering of the AAO films synthesized with two anodization steps in 2 M sulphuric acid, during 1 h, at different temperatures and voltages, was obtained at 5 °C and 20 V (Figure 2c).

If the FFTs of the SEM images of the samples anodized at 10 °C and 20 V in 0.3 M sulphuric acid are compared with the samples anodized at 5 °C and 20 V in 2 M sulphuric acid, a more intense and defined pattern can be observed in the first case, which indicates a higher order. However, in both cases a non-ideal pore arrangement was obtained for the 3 μm^2 analysis area.

3.2. Pore Diameter

Figure 3 shows the variation of the average pore diameter of the nanostructured aluminium oxide films as a function of voltage, sulphuric acid concentration and temperature. A non-significant variation of \overline{dp} with the electrolyte temperature can be observed for samples anodized in 0.3 M sulphuric acid at constant voltage. On the other hand, an increase in \overline{dp} is observed with the increase in the anodization voltage, with significant differences being found for the \overline{dp} obtained at 10 and 20 V.

In the case of AAO films synthesized at different temperatures and voltages in 2 M sulphuric acid a slight tendency of increase in the average pore diameter with the anodization voltage can be seen in Figure 3.

The variation of the pore diameter with the electrolyte concentration was not significant in the range of levels studied, although a slight decrease in \overline{dp} can be seen in Figure 3 with the increase in the concentration of sulphuric acid from 0.3 to 2 M.

These results match with that reported in the literature on a directly proportional dependence of the pore diameter with the synthesis voltage for anodizations carried out in sulphuric acid, independently of the temperature and concentration of the electrolyte [31,34,40].

The best linear regression adjustment to estimate the response of the \overline{dp} as a function of the sulphuric acid concentration, the temperature, and the anodization voltage for the range of experimental levels evaluated is expressed in Equation (2) of Table 1 and explains 99% of the variability in \overline{dp} ($\overline{R}^2 = 0.99$). Although Equation (1) of Table 1 yielded a higher value of \overline{R}^2 , the effects of sulphuric acid concentration and temperature on \overline{dp} were not statistically significant with 95% confidence.

Equation (12), which corresponds to the selected adjustment of Equation (2), with $v = 0.68 \text{ nm/V}$, demonstrates the effect of the anodizing voltage on \overline{dp} , in accordance with observed in Figure 3. These results coincide with those obtained by Sulka and Stepniowski [17], with the variation of \overline{dp} being directly proportional to the anodization voltage for samples anodized in 0.3 and 2 M sulphuric acid, at temperatures between 5 and 30 °C and voltages between 10 and 20 V.

$$\overline{dp} = 0.68 \times V \quad \overline{R}^2 = 0.99 \quad (12)$$

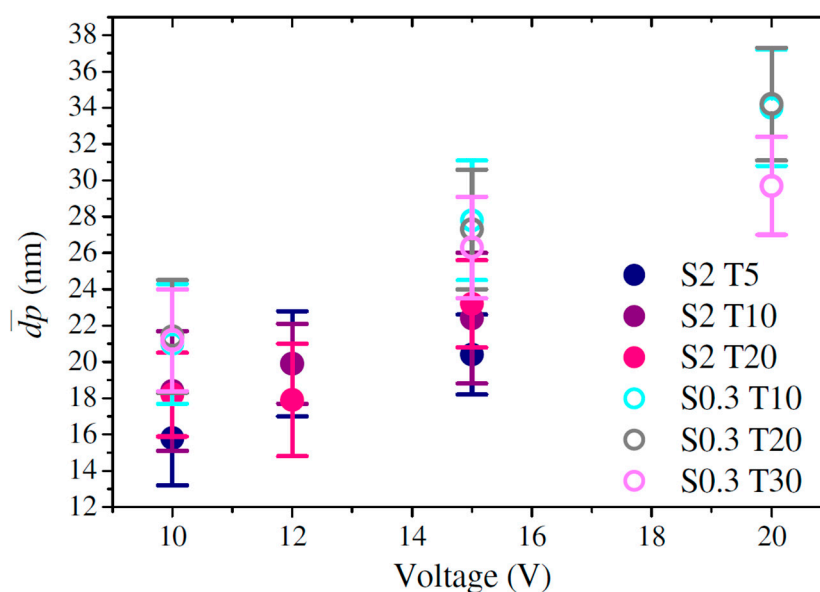


Figure 3. Variation of the average pore diameter of nanostructured aluminium oxide films anodized in sulphuric acid as a function of the concentration and temperature of the electrolyte and the voltage.

3.3. Interpore Distance

Figure 4 shows a variation of the interpore distance directly proportional to the anodization voltage, obtaining a \bar{d}_i close to 28 nm for the samples synthesized at 10 V and 52 nm for the samples synthesized at 20 V, independently of the concentration and temperature of sulphuric acid used in the anodization.

Corresponding to these experimental results, the best linear regression adjustment to predict the interpore distance as a function of the sulphuric acid concentration, the temperature and the anodizing voltage is expressed in Equation (4) of Table 1 and explains 99% of the variability in \bar{d}_i ($\bar{R}^2 = 0.99$). Although the \bar{R}^2 values in Equations (3) and (4) are close to each other, the effect of sulphuric acid concentration and electrolyte temperature can be removed from the model with 95% confidence.

The analysis of Equation (13), which corresponds to the selected adjustment of Equation (4), with $v = 2.66$ nm/V, demonstrates the increase of \bar{d}_i with the increase of the anodization voltage, in agreement with what observed in Figure 4 for the experimental range evaluated. This result coincides with those obtained by Sulka and Parkola [31] in 2 M sulphuric acid for the temperature range -8 to 10 °C and voltages 15–25 V.

$$\bar{d}_i = 2.66 \times V \quad \bar{R}^2 = 0.99 \quad (13)$$

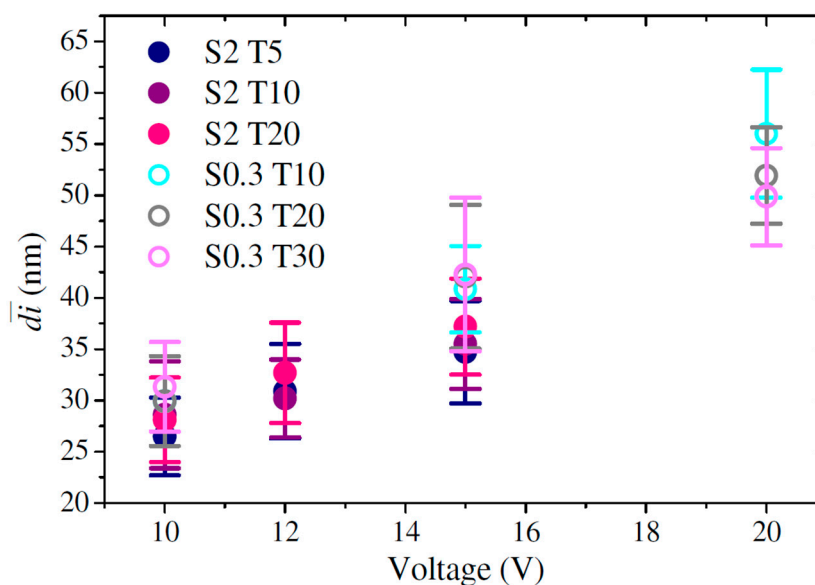


Figure 4. Variation of the average interpore distance of nanostructured aluminium oxide films anodized in sulphuric acid as a function of the concentration and temperature of the electrolyte and the voltage.

3.4. Pore Density

Figure 5 shows a decrease in $\bar{\rho}$ with the increase in the voltage, consequently, to increases in \bar{d}_p and \bar{d}_i . The relationship between $\bar{\rho}$ and the anodization voltage observed in the graph approximates a non-linear behavior, in accordance with the results obtained by Sulka and Stępniewski [17].

For both concentrations of sulphuric acid, a significant effect of the electrolyte temperature on $\bar{\rho}$ is observed in Figure 5. Particularly, at the 0.3 M sulphuric acid concentration, these differences were very slight and occurred at 15 V, between temperatures 10, 20, and 30 °C, whereas, for the 2 M sulphuric acid concentration, these differences were observed for all temperatures, except at 15 V, where an overlap in the error bars was observed for the values of $\bar{\rho}$ obtained at 10 and 20 °C. However, no definite trend was observed with respect to the effect of temperature on $\bar{\rho}$.

On the other hand, a variation of $\bar{\rho}$ with the concentration of sulphuric acid was observed in Figure 5, obtaining the highest pore density values at the highest electrolyte concentration. This could be explained by considering the average pore diameter values for the different concentrations presented in Figure 3. Although no significant differences were observed between the \bar{d}_p at 0.3 and 2 M of sulphuric acid, due to the high dispersion in pore sizes, smaller pore sizes are observed in 2 M sulphuric acid than at the 0.3 M concentration.

The best non-linear regression adjustment to predict pore density as a function of sulphuric acid concentration, temperature and anodization voltage is expressed in Equation (6) in Table 1 and explains 93% of the variability in $\bar{\rho}$ ($\bar{R}^2 = 0.93$). Although Equation (5) presented a value of \bar{R}^2 similar to that Equation (6), the statistical analysis determined a non-significant effect of the temperature variable and therefore, the adjustment equation that does not include this variable was selected.

The analysis of Equation (14), which corresponds to the selected adjustment of Equation (6), with $c = 2.10 \times 10^{10}$ pores/cm² M and $v_2 = 1.08 \times 10^{13}$ pores V²/cm², demonstrates the effect of sulphuric acid concentration and anodization voltage. Thus, the highest values of $\bar{\rho}$ are obtained with the highest concentration values and the lowest voltage values.

$$\bar{\rho} = 2.10 \times 10^{10} \times C + \frac{1.08 \times 10^{13}}{V^2} \quad \bar{R}^2 = 0.93 \quad (14)$$

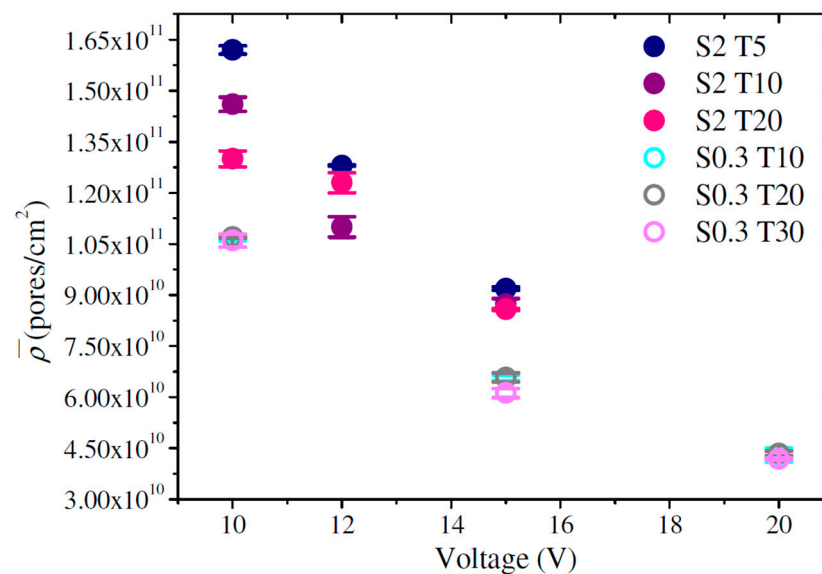


Figure 5. Variation of pore density of nanostructured aluminium oxide films anodized in sulphuric acid as a function of the concentration and temperature of the electrolyte and the voltage.

3.5. Thickness

Figure 6 shows the thickness of the oxide film corresponding to sample S2 T10 V10, using images obtained from the cross-section of the film by optical microscopy and by scanning electron microscopy. In Figure 6b, in addition to observing the substrate and the oxide film, vertical channels of imperfect pore can be identified due to the mechanical treatment performed on the oxide (necessary for thickness measurements in the metallographic optical microscope).

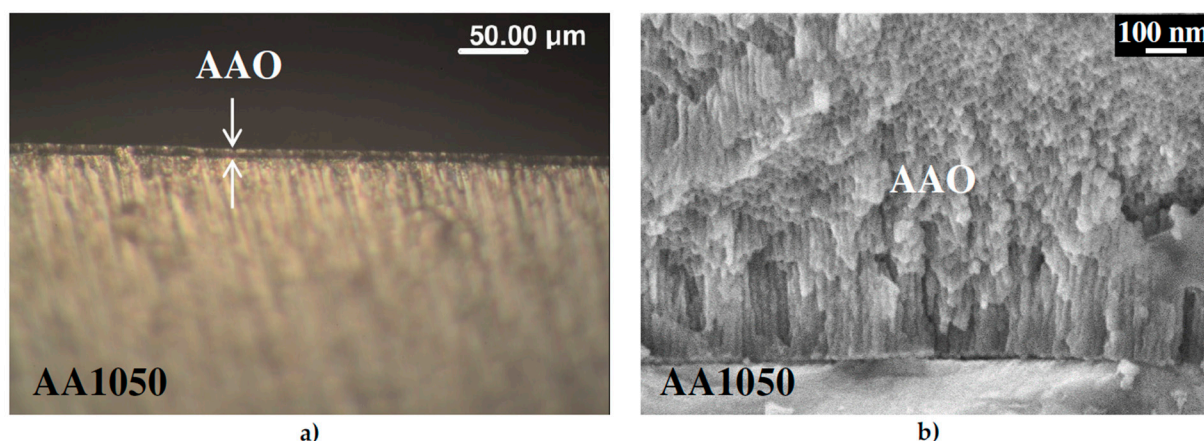


Figure 6. Optical micrograph (a) and scanning electron micrograph (b) of the thickness of the AAO film synthesized in two anodization steps in 2 M sulphuric acid at 10 °C and 10 V for 1 h.

Figure 7 shows an increase in film thickness with the electrolyte temperature and anodization voltage for both sulphuric acid concentrations. Likewise, the increase in thickness is favored at high temperatures and voltages, identifying a synergy for these two variables that explains the deviation from linearity observed in Figure 7, mainly for 20 °C anodized samples in 0.3 and 2 M sulphuric acid.

On the other hand, the thickness of the oxide film increased with the concentration of the electrolyte, favoring the oxide growth process due to a higher concentration of sulphuric acid and the presence of ions in solution. The differences found between the AAO thicknesses obtained at different concentrations were 4 μm for the samples synthesized at 10 V and 10 °C and 13 μm for the samples synthesized at 10 V and 20 °C. At 15 V, these differences were higher at 16 μm at 10 °C and 48 μm at 20 °C. This demonstrates the combined effect of sulphuric acid concentration, temperature, and anodization voltage on the thickness of the anodic oxide film.

The best regression adjustment to estimate the thickness as a function of the sulphuric acid concentration, the temperature and the anodization voltage is expressed in Equation (9) of Table 1, and it explains 49% of the variability in \bar{e} ($\bar{R}^2 = 0.49$), while Equations (7) and (8) submitted an \bar{R}^2 of 0.31 and 0.54, respectively. Although Equation (8) had a higher value of \bar{R}^2 than Equation (9), the latter was selected since the individual effect of temperature and voltage was found to be insignificant and can be removed from the model without significantly affecting the fit.

Equation (15), corresponding to the selected adjustment of Equation (9), with $c = 6.64 \mu\text{m}/\text{M}$ y $tv = 0.05 \mu\text{m}/^\circ\text{C V}$, demonstrates the effect of sulphuric acid concentration and the interaction between temperature and voltage on the thickness of the oxide film, in accordance with that observed in Figure 7.

$$\bar{e} = 6.64 \times C + 0.05 \times T \times V \quad \bar{R}^2 = 0.51 \quad (15)$$

The effect of the synergistic combination of temperature and voltage is highlighted, which allows obtaining oxides of considerable thickness (between 4 and 59 μm) in short times. Thicknesses of the same order were obtained in 14.5 h at low temperatures (1 °C) and voltages between 15 and 20 V [7].

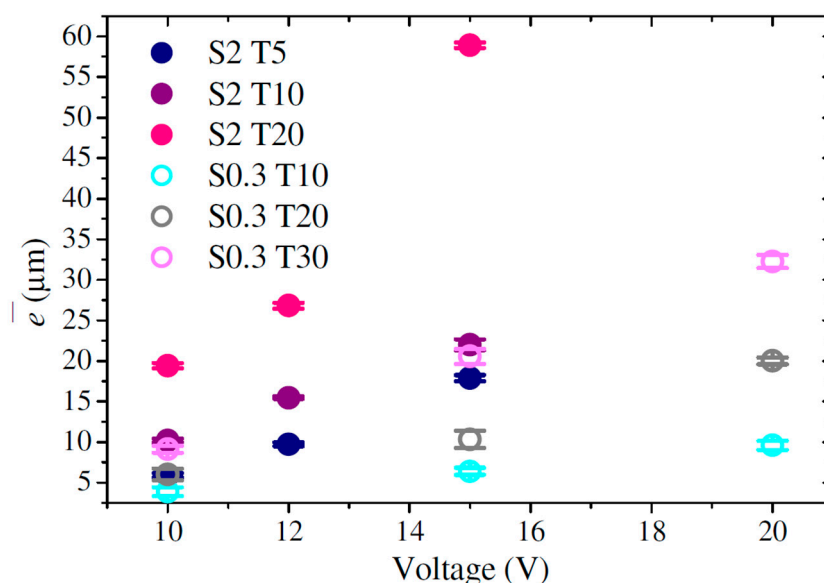


Figure 7. Variation of the average thickness of nanostructured aluminium oxide films anodized in sulphuric acid as a function of the concentration and temperature of the electrolyte and the voltage.

3.6. Porosity

Figure 8 shows the variation of average porosity with voltage, temperature, and sulphuric acid concentration. In general, for all levels of the anodic synthesis variables, nanostructured films with average porosity between 14 and 34% were obtained.

According to Nielsch et al. [36], porosity close to 10% is required for the self-ordering regime of the porous matrix to take place, whatever the anodization conditions. Table 2 shows that the anodization conditions with porosities close to 10% were at 2 M sulphuric acid, 10 V, and 5 and 10 °C; however, under these conditions the best self-orderings were not observed.

For the samples synthesized at 30 °C in 0.3 M sulphuric acid, a decrease of the average porosity with increasing anodization voltage can be observed, while at temperatures of 10 and 20 °C at the same sulphuric acid concentration the variation of \bar{P} with voltage was not significant. This decrease of \bar{P} with the voltage in 0.3 M sulphuric acid at 30 °C could be due to a combination of low pore density (Figure 5) and pore diameter (Figure 3) values compared to the results obtained at 10 and 20 °C. Although it was described above that the pore diameter did not vary significantly with electrolyte temperature due to a large dispersion in pore sizes, the average values revealed lower \bar{d}_p at 30 °C than at 10 and 20 °C.

The opposite was observed in 2 M sulphuric acid, obtaining a significant increase of porosity with increasing anodization voltage for temperatures of 10 and 20 °C (Figure 8). These results are in agreement with those obtained by Chu et al. [2] for one-step anodizations carried out in 2 M sulphuric acid at 8–70 V and 0.1–10 °C. However, at 5 °C, the decrease of \bar{P} with increasing voltage is observed (Figure 8), approximating this result to that observed by Sulka and Parkola [34] for the anodic synthesis range 15–23 V in 2 M sulphuric acid and 1 °C.

On the other hand, the AAO films presented different porosity values with the electrolyte temperature, without the predominance of any trend.

With respect to the electrolyte concentration, a significant effect can be observed at 10 V, with the highest porosity values being obtained in 0.3 M sulphuric acid at 10 and 20 °C.

The best linear regression adjustment for estimating porosity as a function of sulphuric acid concentration, temperature and anodization voltage is expressed in Equation (11) in Table 1 and explains 95% of the variability in \bar{P} ($R^2 = 0.95$). Although Equation (10) presented an \bar{R}^2 close to 95%, the effect of the concentration was not statistically significant.

Equation (16), corresponding to the selected setting of Equation (11), with $t = 0.43 \text{ } ^\circ\text{C}^{-1} \text{ y } v = 1.28 \text{ V}^{-1}$, demonstrates the effect of anodization temperature and voltage on the porosity of the oxide film, in agreement with that observed in Figure 8.

$$\bar{P} = 0.43 \times T + 1.28 \times V \quad \bar{R}^2 = 0.95 \quad (16)$$

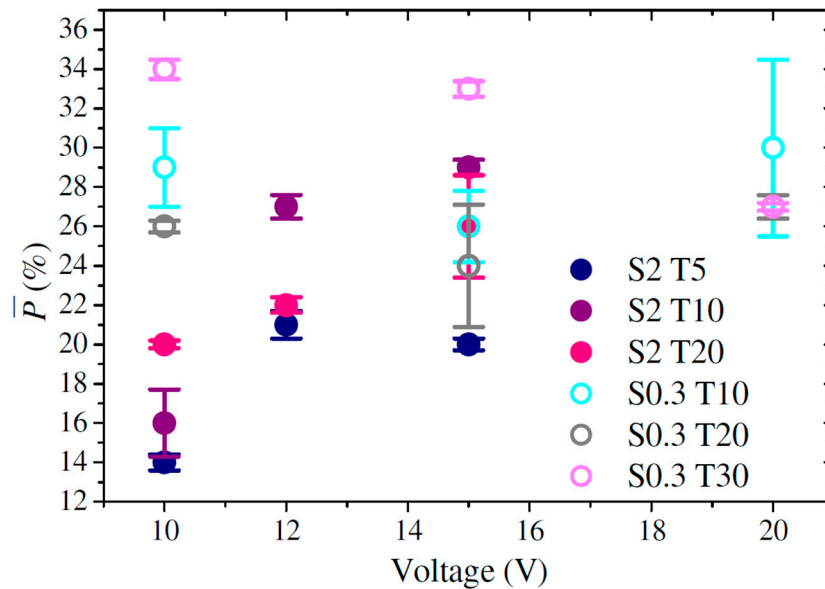


Figure 8. Variation of the average porosity of nanostructured aluminium oxide films anodized in sulphuric acid as a function of the concentration and temperature of the electrolyte and the voltage.

In summary, it was observed that the sulphuric acid concentration influences the pore density and thickness of the OAA films, the anodization voltage on the pore diameter, interpore distance, pore density and porosity, and the temperature on the oxide porosity. A combined effect of voltage and electrolyte temperature on thickness was also observed.

Table 3 presents the results of the morphological parameter adjustments according to the synthesis variables for the range of levels studied using sulphuric acid as electrolyte.

Table 3. Results of adjustments of the morphological parameters according to the synthesis variables. The selected adjustments are highlighted.

Morphological Parameter	Adjustment Equation	Adjustment Parameters					\bar{R}^2 (%)
		c	t	v	v2	tv	
\bar{d}_p	(1.1)	-0.75	0.10	1.62	-	-	98.86
	(2.1)	-	-	1.68	-	-	98.71
\bar{d}_i	(3.1)	-0.70	0.14	2.55	-	-	99.55
	(4.1)	-	-	2.66	-	-	99.45
\bar{p}	(5.1)	2.13×10^{10}	1.97×10^8	-	1.04×10^{13}	-	93.25
	(6.1)	2.10×10^{10}	-	-	1.08×10^{13}	-	93.27
\bar{e}	(7.1)	5.58	0.55	0.22	-	-	31.00
	(8.1)	10.07	-0.73	-0.64	-	0.12	54.18
	(9.1)	6.64	-	-	-	0.05	50.68
\bar{P}	(10.1)	1.12	0.45	1.17	-	-	95.07
	(11.1)	-	0.43	1.28	-	-	95.19

The presented results with sulphuric acid can be compared with those obtained by Bruera et al. [29] using oxalic acid as electrolyte. For example, \bar{d}_p and \bar{d}_i do not depend

only on voltage in oxalic acid, but also on the interaction between voltage and temperature; $\bar{\rho}$ depends on the concentration and voltage as in sulphuric acid and \bar{e} depends on the effect of the three synthesis variables in oxalic acid, in addition to the interaction between temperature and voltage with sulphuric acid. In addition, more ordered pore matrices were obtained in oxalic acid compared to those obtained in sulphuric acid.

Finally, when oxalic acid is used as electrolyte, it is required to control the three synthesis variables in order to obtain a specific morphology; while in anodizations with sulphuric acid, the voltage defines the characteristics of the oxide since it is the main parameter determining the pore diameter and interpore distance.

4. Conclusions

In this work, low-cost anodic aluminium oxide nanostructured coatings were synthesized and characterized from a commercial aluminium alloy by varying the sulphuric acid concentration, temperature, and anodization voltage.

The obtained AAO films presented non-ideal and short-range pore arrangements that changed with the concentration, temperature and synthesis voltage; pore diameters and interpore distances which varied only with anodizing voltage; pore densities that varied with voltage and sulphuric acid concentration; thicknesses that changed significantly with concentration, temperature and voltage, and porosities that varied predominantly with voltage and electrolyte temperature. The key role of voltage on pore dimension when sulphuric acid is used as electrolyte has been demonstrated.

The obtained regression equations explain and allow to predict the relationship between morphological parameters and synthesis variables within the range of the studied conditions. These results lay the foundations for the optimization of resources in the manufacture of nanostructured coatings.

Author Contributions: Conceptualization and methodology, F.A.B. and G.R.K.; software, F.A.B.; formal analysis, F.A.B.; investigation, F.A.B., G.R.K., M.L.V. and A.E.A.; resources, A.E.A.; writing—original draft preparation, F.A.B. and G.R.K.; writing—review and editing, M.L.V. and A.E.A.; supervision, A.E.A.; project administration, A.E.A.; funding acquisition, A.E.A. All authors have read and agreed to the published version of the manuscript.

Funding: This research was funded by Consejo Nacional de Investigaciones Científicas y Técnicas (CONICET) and Agencia Nacional de Promoción Científica y Tecnológica (ANPCyT) of Argentina (PICT-2017-0079), and also funded by the scholarship from CONICET.

Institutional Review Board Statement: Not applicable.

Informed Consent Statement: Not applicable.

Data Availability Statement: The authors confirm that the data supporting the findings of this study are available within the article.

Acknowledgments: We thank the financial support of Consejo Nacional de Investigaciones Científicas y Técnicas (CONICET) and Agencia Nacional de Promoción Científica y Tecnológica (ANPCyT) of Argentina (PICT2017-0079). F. A. Bruera thanks the CONICET for the scholarship granted to carry out this work.

Conflicts of Interest: The authors declare no conflict of interest.

References

1. Sharma, V.P.; Sharma, U.; Chattopadhyay, M.; Shukla, V.N. Advance applications of nanomaterials: A review. *Mater. Today-Proc.* **2018**, *5*, 6376–6380. [[CrossRef](#)]
2. Chu, S.Z.; Wada, K.; Inoue, S.; Isogai, M.; Yasumori, A. Fabrication of Ideally Ordered Nanoporous Alumina Films and Integrated Alumina Nanotubule Arrays by High-Field Anodization. *Adv. Mater.* **2005**, *17*, 2115–2119. [[CrossRef](#)]
3. Jani, A.M.M.; Losic, D.; Voelcker, N.H. Nanoporous anodic aluminium oxide: Advances in surface engineering and emerging applications. *Prog. Mater. Sci.* **2013**, *58*, 636–704. [[CrossRef](#)]
4. Tsangaraki-Kaplanoglou, I.; Theohari, S.; Dimogerontakis, T.; Wang, Y.M.; Kuo, H.H.; Kia, S. Effect of alloy types on the anodizing process of aluminum. *Surf. Coat. Technol.* **2006**, *200*, 2634–2641. [[CrossRef](#)]

5. Santos, A.; Kumeria, T.; Losic, D. Nanoporous anodic aluminum oxide for chemical sensing and biosensors. *Trends Anal. Chem.* **2013**, *44*, 25–38. [[CrossRef](#)]
6. Masuda, H.; Fukuda, K. Ordered metal nanohole arrays made by a two-step replication of honeycomb structures of anodic alumina. *Science* **1995**, *268*, 1466. [[CrossRef](#)] [[PubMed](#)]
7. Sulka, G.D. Highly ordered anodic porous alumina formation by self-organized anodizing. In *Nanostructured Materials in Electrochemistry*; WILEY-VCH: Weinheim, Germany, 2008; Volume 1, pp. 1–11.
8. Bai, A.; Hub, C.C.; Yang, Y.F.; Lin, C.C. Pore diameter control of anodic aluminum oxide with ordered array of nanopores. *Electrochim. Acta* **2008**, *53*, 2258–2264. [[CrossRef](#)]
9. Chi, C.S.; Lee, J.H.; Kim, I.; Oh, H.J. Effects of microstructure of aluminum substrate on ordered nanopore arrays in anodic alumina. *J. Mater. Sci. Technol.* **2015**, *31*, 751–758. [[CrossRef](#)]
10. Poinern, G.E.J.; Ali, N.; Fawcett, D. Progress in nano-engineered anodic aluminum oxide membrane development. *Materials* **2011**, *4*, 487–526. [[CrossRef](#)]
11. Bruera, F.A.; Kramer, G.R.; Vera, M.L.; Ares, A.E. Synthesis and Morphological Characterization of Nanoporous Aluminum Oxide Films by Using a Single Anodization Step. *Coatings* **2019**, *9*, 115. [[CrossRef](#)]
12. Montero-Moreno, J.M.; Sarret, M.; Müller, C. Influence of the aluminum surface on the final results of a two-step anodizing. *Surf. Coat. Technol.* **2007**, *201*, 6352–6357. [[CrossRef](#)]
13. Wu, M.T.; Leu, I.C.; Hon, M.H. Effect of polishing pretreatment on the fabrication of ordered nanopore arrays on aluminum foils by anodization. *J. Vac. Sci. Technol. B Microelectron. Nanometer Struct. Process. Meas. Phenom.* **2002**, *20*, 776–782. [[CrossRef](#)]
14. Wu, M.T.; Leu, I.C.; Hon, M.H. Growth characteristics of oxide during prolonged anodization of aluminum in preparing ordered nanopore arrays. *J. Vac. Sci. Technol. B Microelectron. Nanometer Struct. Process. Meas. Phenom.* **2004**, *22*, 2326–2332. [[CrossRef](#)]
15. Bruera, F.A.; Kramer, G.R.; Vera, M.L.; Ares, A.E. Evaluation of surface pretreatment stages of Al 1050 to obtain nanostructured anodic films. *Superlattices Microstruct.* **2019**, *130*, 103–116. [[CrossRef](#)]
16. Stepniowski, W.J.; Nowak-Stepniowska, A.; Presz, A.; Czujko, T.; Varin, R.A. The effects of time and temperature on the arrangement of anodic aluminum oxide nanopores. *Mater. Charact.* **2014**, *91*, 1–9. [[CrossRef](#)]
17. Sulka, G.D.; Stepniowski, W.J. Structural features of self-organized nanopore arrays formed by anodization of aluminum in oxalic acid at relatively high temperatures. *Electrochim. Acta* **2009**, *54*, 3683–3691. [[CrossRef](#)]
18. Li, A.P.; Müller, F.; Birner, A.; Nielsch, K.; Gösele, U. Fabrication and microstructuring of hexagonally ordered two-dimensional nanopore arrays in anodic alumina. *Adv. Mater.* **1999**, *11*, 483–487. [[CrossRef](#)]
19. Masuda, H. Self-Ordering of Cell Arrangement of Anodic Porous Alumina Formed in Sulfuric Acid Solution. *J. Electrochem. Soc.* **1997**, *144*, L127. [[CrossRef](#)]
20. Kashi, M.A.; Ramazani, A. The effect of temperature and concentration on the self-organized pore formation in anodic alumina. *J. Phys. D Appl. Phys.* **2005**, *38*, 2396. [[CrossRef](#)]
21. Jessensky, O.; Müller, F.; Gösele, U. Self-organized formation of hexagonal pore arrays in anodic alumina. *Appl. Phys. Lett.* **1998**, *72*, 1173–1175. [[CrossRef](#)]
22. Nasirpour, F.; Abdollahzadeh, M.; Almasi, M.J.; Parvini-Ahmadi, N. A comparison between self-ordering of nanopores in aluminium oxide films achieved by two- and three-step anodic oxidation. *Curr. Appl. Phys.* **2009**, *9*, S91–S94. [[CrossRef](#)]
23. Han, X.Y.; Shen, W.Z. Improved two-step anodization technique for ordered porous anodic aluminum membranes. *J. Electroanal. Chem.* **2011**, *655*, 56–64. [[CrossRef](#)]
24. Hurtado, M.J.; Capitán, M.J.; Alvarez, J.; Fatás, E.; Herrasti, P. The Anodic Oxidation of Aluminum: Fabrication and Characterization. *Port. Electrochim. Acta* **2007**, *25*, 153–162. [[CrossRef](#)]
25. Na, H.C.; Sung, T.J.; Yoon, S.H.; Hyun, S.K.; Kim, M.S.; Lee, Y.G.; Shin, S.H.; Choi, S.M.; Yi, S. Formation of unidirectional nanoporous structures in thickly anodized aluminum oxide layer. *Trans. Nonferr. Met. Soc. China* **2009**, *19*, 1013–1017. [[CrossRef](#)]
26. Pardo-Saavedra, D.C.; Londoño-Calderón, C.L.; Menchaca-Nal, S.; Pampillo, L.G.; Martínez García, R.; Socolovsky, L.M. Morphological study of pore widening process in anodized alumina films. *Anal. AFA* **2013**, *25*, 68–71. [[CrossRef](#)]
27. Zaraska, L.; Sulka, G.D.; Szeremeta, J.; Jaskuła, M. Porous anodic alumina formed by anodization of aluminum alloy (AA1050) and high purity aluminum. *Electrochim. Acta* **2010**, *55*, 4377–4386. [[CrossRef](#)]
28. Londoño Calderón, C.L.; Menchaca Nal, S.; Pardo Saavedra, D.C.; Silveyra, J.; Socolovsky, L.M.; Pampillo, L.G.; Martínez García, R. Low cost fabrication of porous anodic alumina: A comparative study of the morphology produced by one- and two-steps of anodization. *Matéria* **2016**, *21*, 677–690.
29. Bruera, F.A.; Kramer, G.R.; Vera, M.L.; Ares, A.E. Evaluation of the influence of synthesis conditions on the morphology of nanostructured anodic aluminum oxide coatings on Al 1050. *Surf. Interfaces* **2020**, *18*, 100448. [[CrossRef](#)]
30. Belwalkar, A.; Grasing, E.; Van Geertruyden, W.; Huang, Z.; Misiolek, W.Z. Effect of processing parameters on pore structure and thickness of anodic aluminum oxide (AAO) tubular membranes. *J. Membr. Sci.* **2008**, *319*, 192–198. [[CrossRef](#)] [[PubMed](#)]
31. Sulka, G.D.; Parkoła, K.G. Temperature influence on well-ordered nanopore structures grown by anodization of aluminium in sulphuric acid. *Electrochim. Acta* **2007**, *52*, 1880–1888. [[CrossRef](#)]
32. Vojkuvka, L.; Marsal, L.F.; Ferré-Borrull, J.; Formentin, P.; Pallarés, J. Self-ordered porous alumina membranes with large lattice constant fabricated by hard anodization. *Superlattices Microstruct.* **2008**, *44*, 577–582. [[CrossRef](#)]
33. Schneider, C.A.; Rasband, W.S.; Eliceiri, K.W. NIH Image to ImageJ: 25 years of image analysis. *Nat. Methods* **2012**, *9*, 671–675. [[CrossRef](#)] [[PubMed](#)]

34. Sulka, G.D.; Parkoła, K.G. Anodising potential influence on well-ordered nanostructures formed by anodisation of aluminium in sulphuric acid. *Thin Solid Films* **2006**, *515*, 338–345. [[CrossRef](#)]
35. O'Sullivan, J.P.; Wood, G.C. The Morphology and Mechanism of Formation of Porous Anodic Films on Aluminium. *Proc. R. Soc. Lond. A* **1970**, *317*, 511–543.
36. Nielsch, K.; Choi, J.; Schwirn, K.; Wehrspohn, R.B.; Gösele, U. Self-ordering regimes of porous alumina: The 10 porosity rule. *Nano Lett.* **2002**, *2*, 677–680. [[CrossRef](#)]
37. Hwang, S.K.; Jeong, S.H.; Hwang, H.Y.; Lee, O.J.; Lee, K.H. Fabrication of Highly Ordered Pore Array in Anodic Aluminum Oxide. *Korean J. Chem. Eng.* **2002**, *19*, 467–473. [[CrossRef](#)]
38. Ebihara, K.; Takahashi, H.; Nagayama, M. Interpretation of the voltage-current characteristics observed when anodizing aluminum in acid solutions. *Kinzoku Hyomen Gijutsu* **1984**, *35*, 205–209.
39. Wood, G.C.; O'Sullivan, J.P. The anodizing of aluminium in sulphate solutions. *Electrochim. Acta* **1970**, *15*, 1865–1876. [[CrossRef](#)]
40. Myung, N.V.; Lim, J.; Fleurial, J.-P.; Yun, M.; West, W.; Choi, D. Alumina nanotemplate fabrication on silicon substrate. *Nanotechnology* **2004**, *15*, 833. [[CrossRef](#)]